Heat Mass Transfer (2016) 52:2781–2794
DOI 10.1007/s00231-016-1776-7

ORIGINAL

Assessment of zero-equation SGS models for simulating indoor environment

Javad Taghinia[1,2] · Md Mizanur Rahman[1] · Tim K.T. Tse[2]

Received: 5 August 2015 / Accepted: 8 February 2016 / Published online: 25 February 2016

Abstract The understanding of air-flow in enclosed spaces plays a key role to designing ventilation systems and indoor environment. The computational fluid dynamics aspects dictate that the large eddy simulation (LES) offers a subtle means to analyze complex flows with recirculation and streamline curvature effects, providing more robust and accurate details than those of Reynolds-averaged Navier–Stokes simulations. This work assesses the performance of two zero-equation sub-grid scale models: the Rahman–Agarwal–Siikonen–Taghinia (RAST) model with a single grid-filter and the dynamic Smagorinsky model with grid-filter and test-filter scales. This in turn allows a cross-comparison of the effect of two different LES methods in simulating indoor air-flows with forced and mixed (natural + forced) convection. A better performance against experiments is indicated with the RAST model in wall-bounded non-equilibrium indoor air-flows; this is due to its sensitivity toward both the shear and vorticity parameters.

List of symbols

C_μ	Eddy-viscosity coefficient
C_s	Smagorinsky coefficient
G	Filter function
g	Gravitational acceleration
k	Total turbulent kinetic energy
L_{ij}	Leonard stress
Pr	Molecular Prandtl number
Pr_{sgs}	Sub-grid scale Prandtl number
Re	Reynolds number
$\bar{S}_{ij}$	Resolved strain-rate tensor
T	Temperature
$\bar{u}_i$	Grid-filter velocities
$\tilde{\bar{u}}_i$	Test-filter velocities
$\bar{u}_\tau$	Friction velocity
$\overline{W}_{ij}$	Resolved vorticity tensor
y^+	Dimensionless wall distance ($\bar{u}_\tau y/\nu$)
β	Thermal expansion coefficient
$\delta_{i,j}$	Kronecker's delta
Δt	Time step
$\bar{\Delta}$	Grid-filter width
$\tilde{\Delta}$	Test-filter width
ν, ν_T	Laminar and turbulent viscosities
$\bar{\theta}_j$	Grid-filter temperature
$\tilde{\bar{\theta}}_i$	Test-filter temperature
ρ	Density
$\tau_{i,j}$	Sub-grid scale stress tensor

Abbreviations

CFD	Computational fluid dynamics
DSM	Dynamic Smagorinsky model
LES	Large eddy simulation
RANS	Reynolds averaged Navier–Stokes
RAST	Rahman–Agarwal–Siikonen–Taghinia
SGS	Sub-grid scale

Subscript

i, j	Variable numbers
in	Inlet condition
out	Outlet condition

✉ Javad Taghinia
taghinia.j@gmail.com

[1] Department of Mechanical Engineering, Aalto University, Espoo, Finland

[2] Department of Civil and Environmental Engineering, Hong Kong University of Science and Technology, Hong Kong SAR, China

1 Introduction

An optimum air-distribution system has a vital impact on the health of occupants, comprising a pivotal factor in energy conservation concerning the building aspects. Therefore, designing a comfortable and efficient indoor environment needs a proper understanding of the air velocity, temperature distribution and turbulent characteristics of the flow. There are a few strategies to drive the air inside an enclosed space, such as forced and mixed convection flows which can be achieved via an external air-supply system, invoking a complex flow structure. Consequently, it is very challenging to predict the complete physics of an indoor air-flow.

Experimental works can provide a good insight into the structure of the air-flow but they need a full scale testing to achieve this goal. They are also costly and time consuming, and cannot be applied to different cases. In recent decades, the computational fluid dynamics (CFD) approach which is to be the complement of experimental and theoretical methods, has gained an increased attention due to its robustness and cost-effectiveness. The CFD simulation provides a detailed information on relevant parameters such as velocity fluctuations, thermal distribution and jet-spread rate in indoor environments. One of the most common CFD approaches in an indoor air-flow is the Reynolds averaged Navier–Stokes (RANS) modeling. This method has gained a popularity due to its robustness and economic computing resources. The RANS requires a coarse grid as well as less computational time compared with other available approaches. However, it has a few drawbacks especially in indoor air-flow simulations. One of these limitations is that the RANS utilizes an averaging procedure, making it incapable of providing instantaneous information concerning turbulent structures which have a vital importance for the thermal-comfort optimization. Another drawback concerns the performance of RANS models; as there are many variants of RANS turbulence models, such as the one-equation model, two-equation model and second-moment model which may produce good results for one case but perform poorly in another one [1]. Therefore, the accuracy of results is under question, making it a difficult task for the designer to choose a suitable and reliable approach. The performance of the various RANS turbulence models has been investigated by many authors [1–8] in the literature.

Large eddy simulation (LES) can be an alternative approach to modeling an enclosed space air-flow. However, an LES needs a finer grid resolution and higher computational time compared with the RANS. Since the LES calculates the time-dependent flow, it is capable of providing a detailed information on turbulence properties and velocity fluctuations. The air-flow in the building has a turbulent nature, containing separation and recalculation regions that dramatically affect the indoor air quality. The LES can predict these structures in a more accurate sense by considering an extra-ordinary procedure to capture most of the turbulent structures in a wide range of scales. Considering these facts, the LES can be a better solution to the indoor air-flow simulation than the RANS.

An LES decomposes the flow field into two types of eddy structures, namely the large scale and sub-grid scale (SGS). Large eddies are solved directly while the small ones are modeled. The SGS eddies are nearly isotropic and they are independent of the flow geometry and have a universal behavior. Therefore, the SGS model deals with a few empirical coefficients when compared with an RANS modeling.

Since the last three decades, various SGS models have been developed; Smagorinsky [9] and dynamic Smagorinsky [10] models are among the most popular ones. The Smagorinsky model (SM) benefits from a constant eddy-viscosity coefficient which is simple and robust, but not suitable for complex flows in which the coefficient changes with time and space. On the other hand, the dynamic Smagorinsky model (DSM) calculates the eddy-viscosity coefficient locally by considering the flow properties varying with time and space. Since the DSM uses two filtering procedures, it is difficult to implement and is not as robust as the Smagorinsky model, especially for a more complex air-flow [11]. There have been a lot of efforts for introducing new models based on the constrained variational approach [12] or the Lagrangian dynamic model [13]. However, they need additional parameters to be calculated, resulting in a challenging task to apply them for wall-bounded flows.

The Rahman–Agarwal–Siikonen–Taghinia (RAST) model with a variable eddy-viscosity coefficient is recently developed by Taghinia et al. [14]; this parameter preserves the anisotropic characteristics of turbulence in the sense that it is sensitized to non-equilibrium flows. It provides a natural damping of the eddy-viscosity as the solid-wall is approached. It is worth mentioning that the SM has a few drawbacks that limit its applications to selected fluid flow problems. One of these shortcomings is that the model needs an empirical constant which varies for different flow problems. The second shortcoming is its inability in producing the required damping of the eddy-viscosity in the near-wall region. The disadvantages of DSM are: the model coefficient has large variations in fairly small regions of the flow; produces large negative values of eddy-viscosity (something like “back-scatter”) that cause numerical instability; too much reliance on smallest scales which are not accurately simulated, i.e., noisy and the total viscosity (laminar viscosity + eddy-viscosity) is equated to zero whenever negative, called clipping; requires statistical homogeneity for averaging. However, unlike the DSM, the RAST model does not rely on assumptions of

statistical homogeneity for averaging and indulges in no clipping operations. This model needs only a single filter, making it more robust for use in majority of fluid flow problems. In addition, it requires no *ad-hoc* strategies for achieving the numerical stabilization. Finally, one can save some computational effort in the proposed model, since the test-filtering operation on the SGS stress is not required. In other words, the current model can be considered as a good compromise between accuracy and manageability; particularly, as simple as the original SM and as accurate as the DSM.

The motivation of this current study is to assess the potentiality of both the RAST model and DSM in simulating the dynamics of an indoor air-flow supported by measurements. Three indoor air-flow cases are calculated: the first and second cases deal with forced and mixed convection, respectively, in a room; the third case focuses on the flow structure in a room subjected to an air-flow, injected from a duct impinging on the floor. These three scenarios provide a good benchmark to test the performance of turbulence models in various conditions, which are common to the room-air ventilation.

2 Large eddy simulation (LES)

The LES model has been developed by Smagorinsky [9]. In an LES, the largest eddies that contain the major fraction of energy are computed whereas the small eddies are modeled. This process is performed by applying a filter function $G(x;x')$ to a decomposed function f:

$$f = \bar{f} + f_{sgs}, \quad \bar{f} = \int_{R^3} G(x;x') f(x') dx' \tag{1}$$

where the function f is decomposed to resolved (i.e., averaged) and sub-grid scale values. The implied filter function $G(x;x')$ herein, operated on a filter width $\bar{\Delta}$ is a top-hat filter. Applying the spatial filter to incompressible Navier–Stokes equations and using the commutation characteristics, the LES equations yield:

$$\frac{\partial \bar{u}_j}{\partial x_i} = 0 \tag{2}$$

$$\frac{\partial \bar{u}_i}{\partial t} + \frac{\partial \bar{u}_i \bar{u}_j}{\partial x_j} = -\frac{1}{\rho}\frac{\partial \bar{p}}{\partial x_i} + \frac{\partial}{\partial x_j}\left(\nu \frac{\partial \bar{u}_i}{\partial x_j}\right) - \frac{\partial \tau_{ij}}{\partial x_j} + g_j \beta \left(\bar{\theta} - \theta_0\right)\delta_{ij} \tag{3}$$

where the sub-grid scale (SGS) stress tensor is defined as

$$\tau_{ij} = \overline{u_i u_j} - \bar{u}_i \bar{u}_j \tag{4}$$

The filtered energy equation is:

$$\frac{\partial \bar{\theta}}{\partial t} + \frac{\partial \bar{u}_j \bar{\theta}}{\partial x_j} = \frac{\partial}{\partial x_j}\left(\frac{\nu}{Pr}\frac{\partial \bar{\theta}}{\partial x_j}\right) - \frac{\partial h_j}{\partial x_j} \tag{5}$$

where the sub-grid heat fluxes are given by

$$h_j = \overline{u_j \theta} - \bar{u}_j \bar{\theta} \tag{6}$$

The sub-grid Reynolds stresses and heat fluxes are unknown and need to be modeled.

2.1 RAST sub-grid scale model

The RAST model with a single grid filter is recently developed for the large eddy simulation [14]. In this sub-grid scale (SGS) model, the unknown SGS turbulent stresses resulting from the filtering operation in Eq. (4) need a closure. Following the Boussinesq approximation, the relationship between the anisotropic part of the SGS stress tensor and the large-scale (i.e., resolved) strain-rate tensor can be expressed as:

$$\tau_{ij} - \frac{1}{3}\delta_{ij}\tau_{kk} = -2\nu_T \bar{S}_{ij}, \quad \bar{S}_{ij} = \frac{1}{2}\left(\frac{\partial \bar{u}_i}{\partial x_j} + \frac{\partial \bar{u}_j}{\partial x_i}\right) \tag{7}$$

The isotropic part of stress tensor ($\frac{1}{3}\delta_{ij}\tau_{kk}$) is implicitly added to the pressure. The SGS eddy-viscosity ν_T is a scalar quantity and is determined as:

$$\nu_T = C_\mu \, \bar{\Delta}^2 \, \bar{S} \tag{8}$$

where C_μ is a model coefficient, $\bar{S} = \sqrt{2\bar{S}_{ij}\bar{S}_{ij}}$ is the invariant of resolved strain-rate tensor, and $\bar{\Delta}$ is the grid-filter length (or width) computed from the cell-volume:

$$\bar{\Delta} = (\Delta_1 \Delta_2 \Delta_3)^{\frac{1}{3}} \tag{9}$$

where Δ_1, Δ_2 and Δ_3 are the grid sizes in x, y and z directions, respectively. The eddy-viscosity coefficient C_μ appearing in Eq. (8) is an indisputably flow-dependent quantity which can be readily computed as a scalar function of the invariants formed on the resolved strain-rate $\bar{S}_{ij}$ tensor and the resolved vorticity tensor given by

$$\overline{W}_{ij} = \frac{1}{2}\left(\frac{\partial \bar{u}_i}{\partial x_j} - \frac{\partial \bar{u}_j}{\partial x_i}\right) \tag{10}$$

The invariants of resolved strain-rate and vorticity tensors are defined by $S = \sqrt{2\bar{S}_{ij}\bar{S}_{ij}}$ and $W = \sqrt{2\bar{W}_{ij}\bar{W}_{ij}}$, respectively.

The SGS turbulent kinetic energy k_{sgs} transport model accounts for the history and non-local effects, having the potential to benefit the modeling of complex flows with non-equilibrium turbulence. The SGS kinetic energy is defined as:

$$k_{sgs} = \frac{1}{2}\tau_{kk} = \frac{1}{2}(\overline{u_k u_k} - \bar{u}_k \bar{u}_k) \tag{11}$$

which can be obtained by contracting the sub-grid scale stress in Eq. (4). However, with the RAST model k_{sgs} is computed algebraically as:

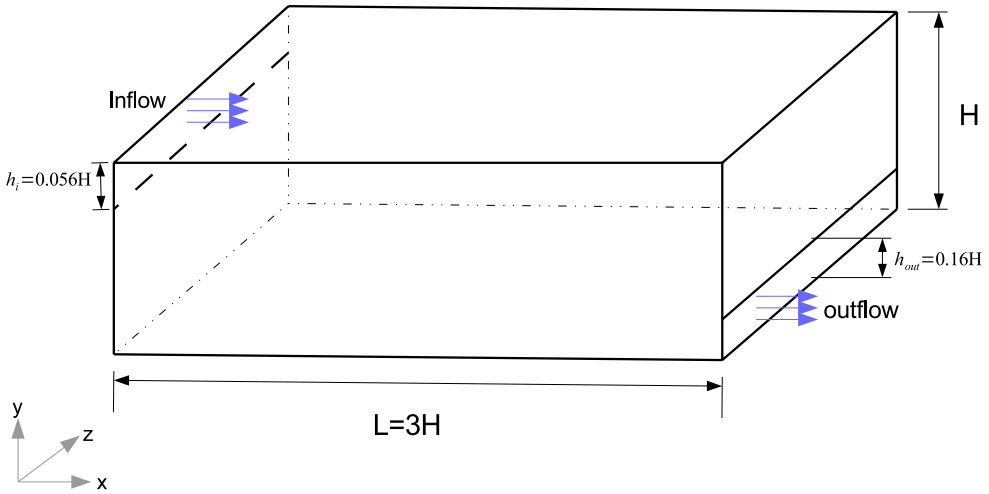

Fig. 1 Computational domain for forced convection case

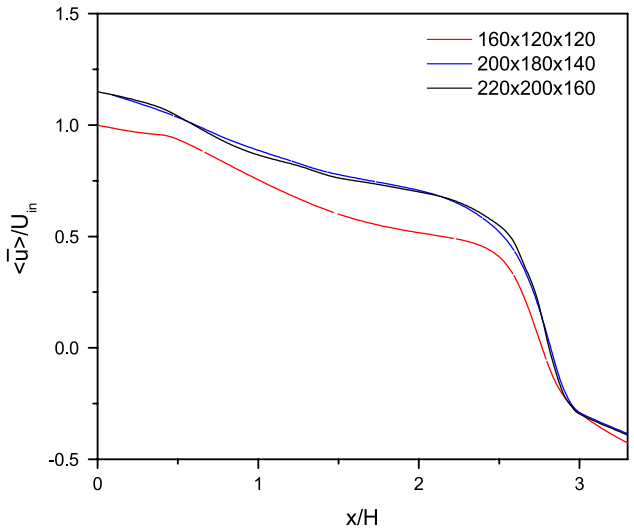

Fig. 2 Effect of grid density on mean velocity magnitude at $y/H = 0.972$ for forced convection

$$k_{sgs} = C_{\bar{\mu}}^{\frac{2}{3}} (\bar{\Delta}\bar{S})^2 \tag{12}$$

The formulation for C_μ as suggested by Rahman and Siikonen [15] in RANS modeling is adapted with the RAST model:

$$C_\mu = \frac{1}{2\left(1 + T_t \bar{S}\sqrt{1+\Re^2}\right)} \tag{13}$$

where T_t is the hybrid time scale calculated as:

$$T_t = \sqrt{\frac{k^2}{\epsilon^2} + C_T^2 \frac{\nu}{\epsilon}} = \frac{k}{\epsilon}\sqrt{1 + \frac{C_T^2}{Re_T}}, \quad Re_T = \frac{k^2}{\nu\,\epsilon} \tag{14}$$

where Re_T is the turbulent Reynolds number. Equation (14) guarantees that the eddy time scale never falls below the Kolmogorov time scale $C_T\sqrt{\nu/\epsilon}$, which is dominant in the immediate neighborhood of the solid wall. Alternatively, the turbulence time scale is k/ϵ at a large Re_T but approaches the Kolmogorov limit $C_T\sqrt{\nu/\epsilon}$ for $Re_T \ll 1$. The empirical constant $C_T = \sqrt{2}$ associated with the Kolmogorov time scale is estimated from the behavior of k-transport equation in the RANS modeling as given in Reference [16]. In the viscous sublayer $k = y^2/(C_T^2\nu/\epsilon)$, where the basic scale is the Kolmogorov time scale and y is the normal distance from the wall. Besides, the k-equation reduces to $\nu\partial^2 k/\partial y^2 = \epsilon$ as the wall is approached. Combining these two relations gives $C_T = \sqrt{2}$. In Eq. (13), $\Re = \left|\overline{W}/\bar{S}\right|$ is a dimensionless parameter which is very useful in characterizing the flow. Therefore, the flow-dependent C_μ is appropriate for both the shear and vorticity dominated flows that are far from equilibrium. It is worth mentioning that the strain-dependent coefficient C_μ in the eddy-viscosity equation provides natural damping as the wall is approached. This feature has its significance in flows with separation and reattachment.

To this end, it can be stressed that the WALE [17, 18] models based on the invariant of resolved strain-rate tensor, in particular, retain the eddy-viscosity approach and modify the Smagorinsky model to allow for an adaptation of its structure with the flow. Their modification of the model coefficient C_μ is similar to the one proposed in the current model. Nevertheless, the glaring difference is that the WALE and Vreman models additionally invoke flow-dependent constants with C_μ in contrast to the present model.

The total kinetic energy k and the dissipation ϵ are determined by the expressions:

$$k = k_{sgs} + \frac{1}{2}\bar{u}_k'\bar{u}_k', \quad \epsilon = 2(\nu + \nu_T)\bar{S}_{ij}\bar{S}_{ij} \tag{15}$$

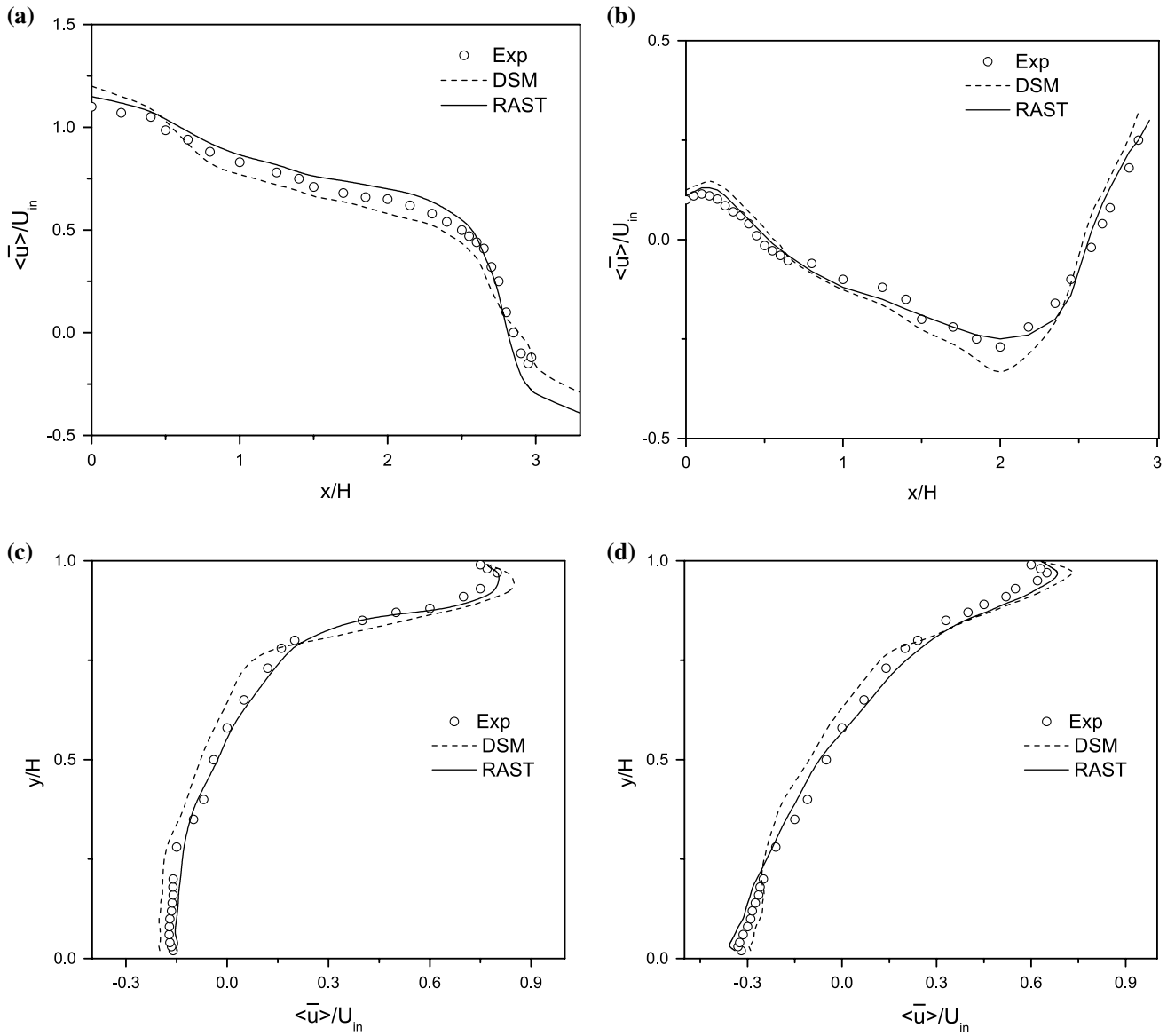

Fig. 3 Mean velocity profiles at different locations for forced convection. **a** $y/H = 0.972$, **b** $y/H = 0.028$, **c** $x/H = 1$, **d** $x/H = 2$

where $(\bar{u}'_k \bar{u}'_k/2)$ is the resolved turbulent kinetic energy. The sub-grid heat fluxes are modeled using the gradient-transport hypothesis as:

$$h_j = \alpha_{sgs} \frac{\partial \bar{\theta}}{\partial \bar{u}_j}, \quad \alpha_{sgs} = \frac{\nu_{sgs}}{Pr_{sgs}} \tag{16}$$

where $Pr_{sgs} = 0.5$ is assumed.

2.2 Dynamic Smagorinsky model (DSM)

To avoid the drawbacks inherited by the Smagorinsky model (SM), a dynamic version of this SM is used in the current study. The SM based on the isotropic eddy-viscosity ν_T computes the SGS stresses from:

$$\tau_{ij} - \frac{1}{3}\delta_{ij}\tau_{kk} = -2\nu_T \bar{S}_{ij} = 2\bar{C}_s \bar{\Delta}^2 |\bar{S}| \bar{S}_{ij} \tag{17}$$

where $\bar{C}_s$ is a Smagorinsky constant. This model boasts of being in simplicity, economy and robustness. However, it has several well-known shortcomings. The most problematic aspect of the model from a practical standpoint is that there is no single value for $\bar{C}_s$ which is universally applicable to a wide range of flows. In addition, the energy dissipation in this model is generally too high in regions where the laminarization of flow can occur along with the mean

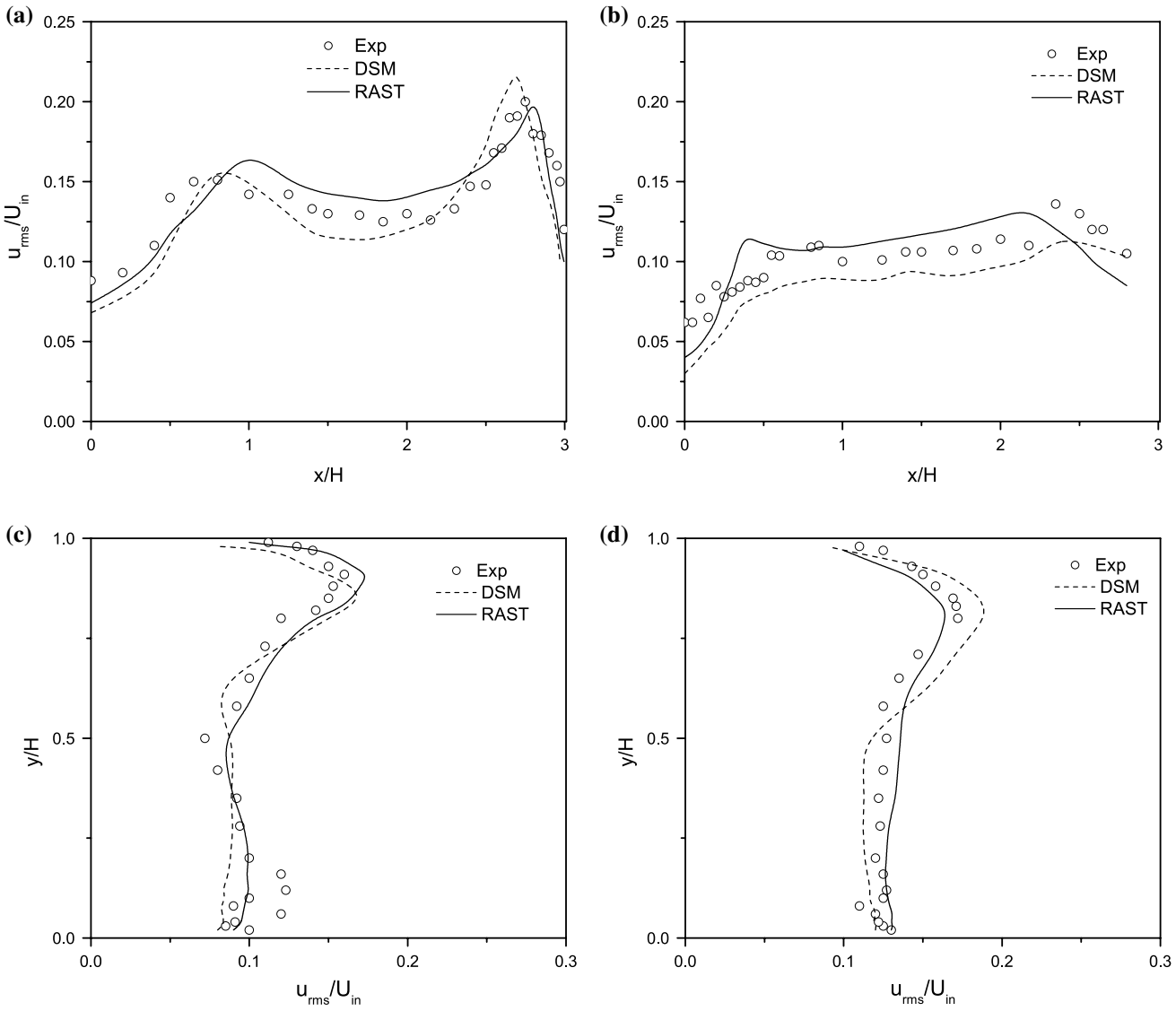

Fig. 4 RMS fluctuating velocity profiles at different locations for forced convection. **a** $y/H = 0.972$, **b** $y/H = 0.028$, **c** $x/H = 1$, **d** $x/H = 2$

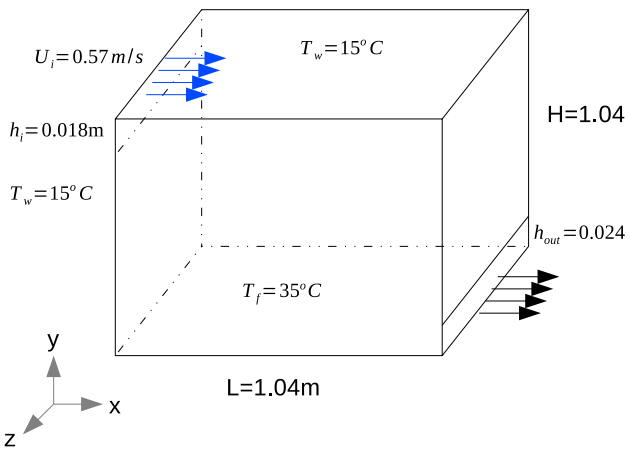

Fig. 5 Computational domain for mixed convection

shear, and it has a low correlation with the actual turbulent stress tensor [10]. In other words, it is not a particularly good representation of small-scale turbulence. This point has been reinforced by simulation results near solid boundaries that show significant errors [19].

Germano et al. [10] and subsequently Lilly [20] developed a method to calculate a dynamic $\bar{C}_s$ according to local flow characteristics by adding another filter, called the test-filter $\tilde{G}$ (a tilde denotes the test-filtering operation at the test-filter scale). The grid scale of this test-filter is denoted by $\tilde{\Delta} = \alpha\bar{\Delta}$; because the test-filter width $\tilde{\Delta}$ must be greater than the grid-filter width $\bar{\Delta}$, i.e., $\alpha > 1$. The Germano identity requires that:

$$L_{ij} = T_{ij} - \tilde{\tau}_{ij} = \widetilde{\bar{u}_i\bar{u}_j} - \tilde{\bar{u}}_i\tilde{\bar{u}}_j - \left(\widetilde{\bar{u}_i\bar{u}_j} - \widetilde{\bar{u}_i}\widetilde{\bar{u}_j}\right) = \widetilde{\bar{u}_i}\widetilde{\bar{u}_j} - \tilde{\bar{u}}_i\tilde{\bar{u}}_j \tag{18}$$

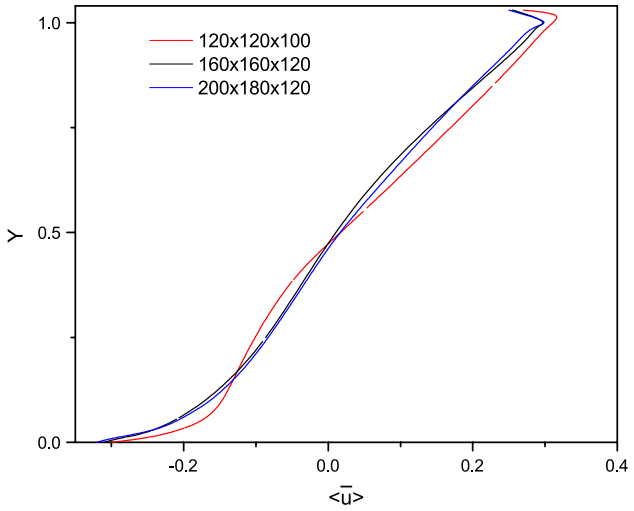

Fig. 6 Effect of grid density on mean velocity magnitude at $x/L = 0.5$ for mixed convection

where T_{ij} is the SGS stress on the test-filter level. The stress components L_{ij} can be interpreted as the stress associated with the smallest resolved scales between the test-filter scale ($\tilde{\Delta}$) and the grid-filter scale ($\bar{\Delta}$). The stress tensor L_{ij} is called the Leonard stress and can be directly computed from the resolved scales.

If $\bar{C}_s$ is assumed not to be changed significantly from the grid-filter to the test-filter scales, the error generated by using the Smagorinsky model in the Germano identity is:

$$E = L_{ij} - \frac{\delta_{ij}}{3} L_{kk} - \bar{C}_s M_{ij}, M_{ij} = 2\bar{\Delta}^2 \left(\widetilde{|\bar{S}|\bar{S}_{ij}} - \alpha^2 \eta |\tilde{\bar{S}}| \tilde{\bar{S}}_{ij} \right) \quad (19)$$

with $\eta = \tilde{C}_s / \bar{C}_s$. Generally $\alpha = 2$ and the scale variance ($\eta = 1$) is assumed. Following Lilly's idea [20], the model coefficient $\bar{C}_s$ is obtained by seeking for $\bar{C}_s$ which minimizes the square of the error E^2. Therefore, taking $\partial E^2 / \partial \bar{C}_s$ and setting it to zero gives

$$\bar{C}_s = \frac{L_{ij} M_{ij}}{M_{ij} M_{ij}} \quad (20)$$

The model coefficient $\bar{C}_s$, thus obtained is a local quantity, varying in time and space in a fairly wide range having positive and negative values. Although a negative $\bar{C}_s$ (and therefore a negative ν_T) is often interpreted as the flow of energy from the sub-grid scale eddies to the resolved eddies (referred to as "back-scatter") and regarded as a desirable attribute of the dynamic model, too large a negative ν_T causes numerical instability, leading to divergence of the numerical solution. To avoid this, $\bar{C}_s$ is simply clipped at zero.

In particular, the Prandtl number of DSM can be determined as suggested by Lilly [20]:

$$\frac{1}{Pr_{sgs}} = \frac{1}{\bar{C}_s} \frac{P_j R_j}{R_j R_j} \quad (21)$$

where

$$P_j = \widetilde{\bar{u}_j \bar{\theta}} - \tilde{\bar{u}}_j \tilde{\bar{\theta}}, \qquad R_j = 2\bar{\Delta}^2 \left(\widetilde{|\bar{S}| \frac{\partial \bar{\theta}}{\partial x_j}} - \alpha^2 \eta |\tilde{\bar{S}}| \frac{\partial \tilde{\bar{\theta}}}{\partial x_j} \right) \quad (22)$$

This model has successfully predicted a fully developed turbulent channel flow.

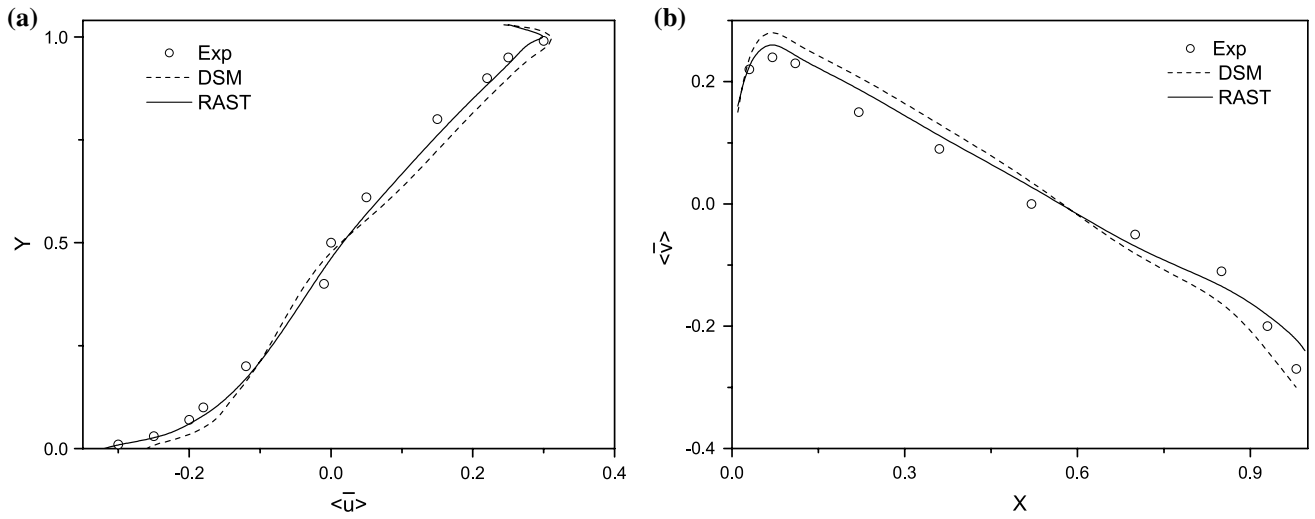

Fig. 7 Mean velocity profiles at different locations for mixed convection. **a** $x/L = 0.5$, **b** $y/L = 0.5$

3 Computational aspects

The filtered incompressible Navier–Stokes equations are integrated on a collocated grid using a finite-volume method. The continuity and momentum equations are coupled using the SIMPLE (semi-implicit method for pressure-linked equations) algorithm. A modified Rhie–Chow interpolation is used for the pressure gradient terms to avoid pressure oscillations due to the collocated grid arrangement [21, 22]. A second-order upwind flux-difference splitting scheme for convective terms and a central differencing scheme for diffusion terms are applied. For time integration, a Crank–Nicolson second-order accurate scheme is used. An algebraic multi-grid method is employed to accelerate the solution convergence. The present numerical method and the associated solver have been tested extensively by computing several laminar and turbulent flows [23–25].

To validate the performance of a recently developed zero-equation model RAST [14] in an indoor airflow, three ventilation cases with a forced convection, a mixed convection and an isothermal impinging-jet in a room are considered. Each case is discussed in its devoted section and results are compared with available experimental data. To evaluate the generality and accuracy of RAST model, computations are compared with those obtained using the DSM [10, 20]. Presumably, the influence of the sub-grid

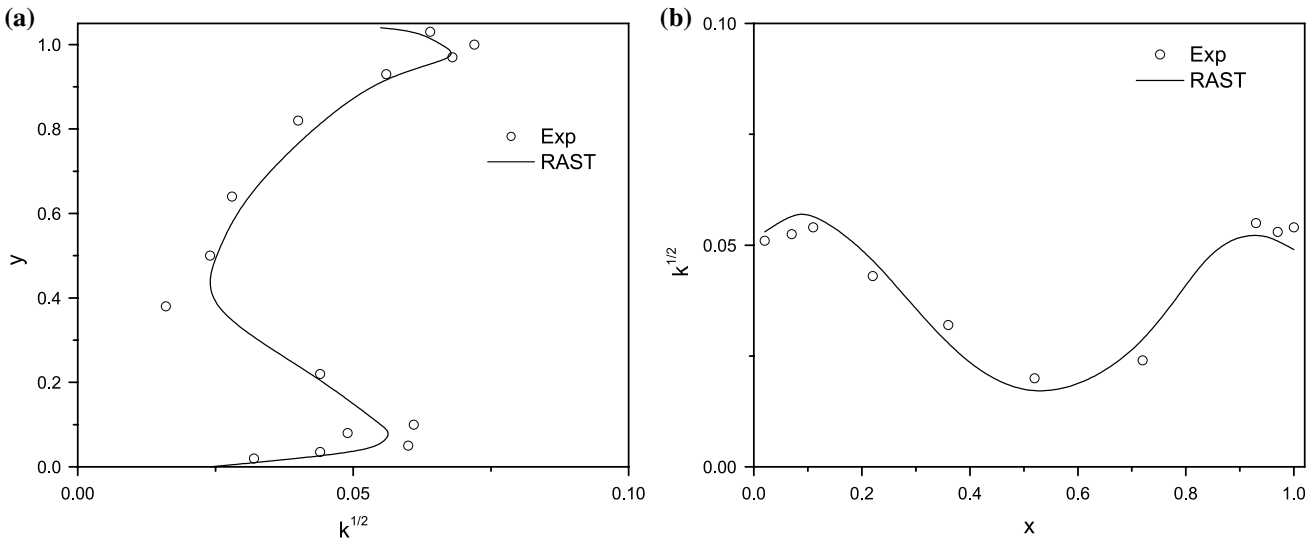

Fig. 8 Turbulent kinetic profiles at different locations for mixed convection. **a** $x/L = 0.5$, **b** $y/L = 0.5$

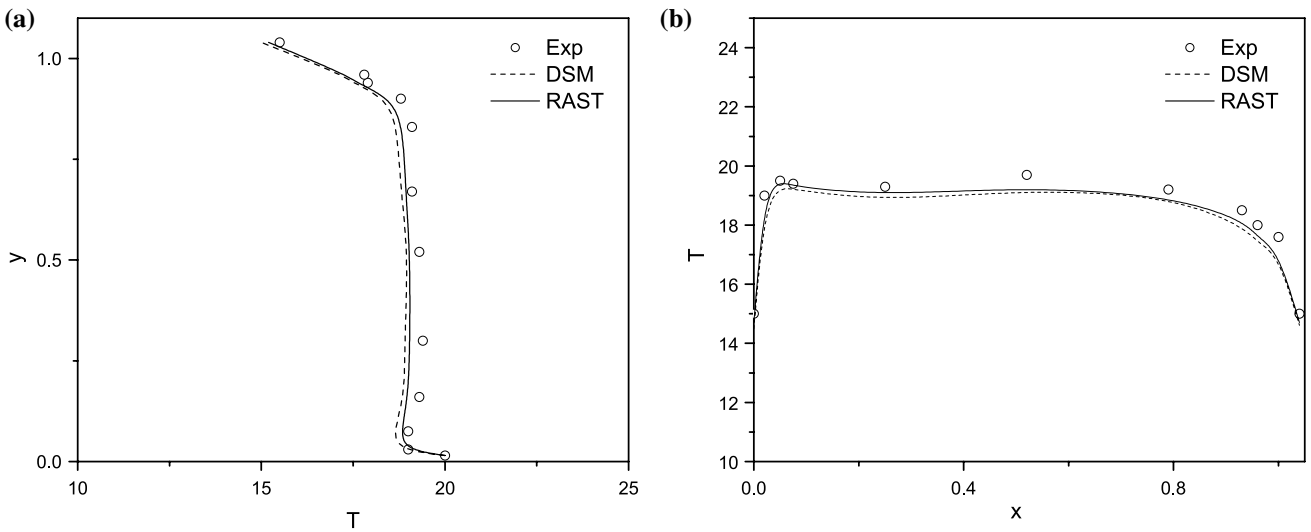

Fig. 9 Mean temperature profiles at different locations for mixed convection. **a** $x/L = 0.5$, **b** $y/L = 0.5$

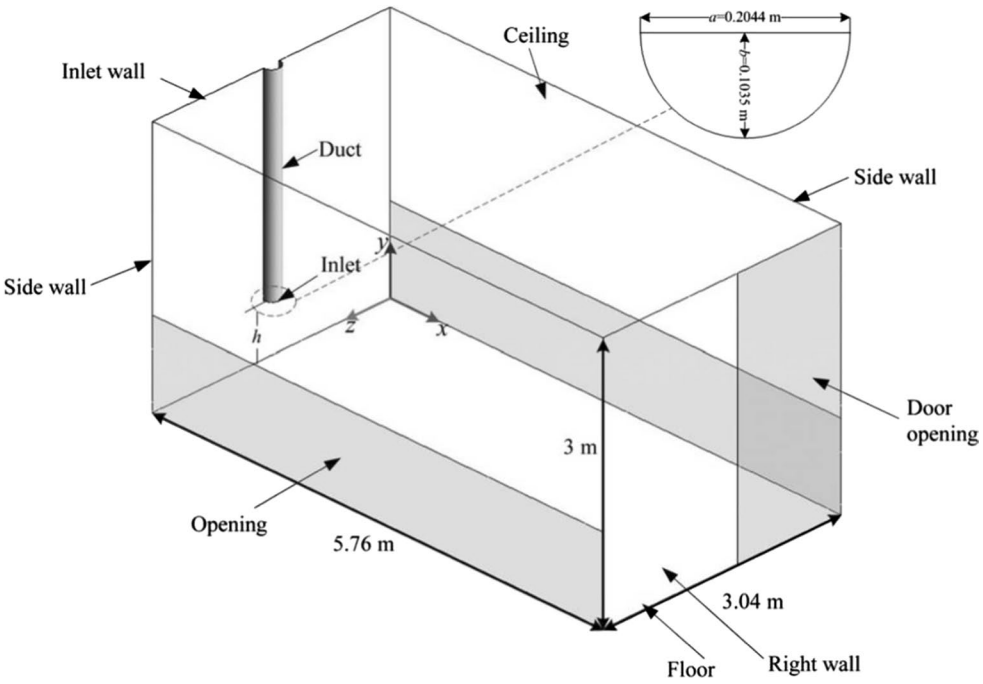

Fig. 10 Computational domain for impinging jet in a room

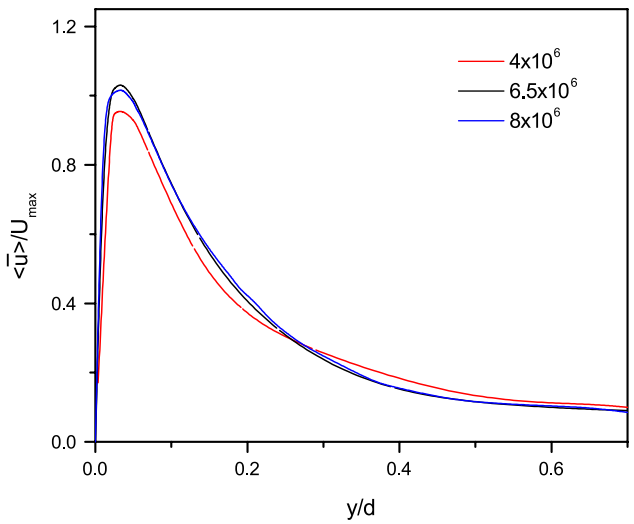

Fig. 11 Effect of grid density on mean velocity magnitude at $x = 0.3$ m for impinging jet in a room

model on the results should be significant on the employed meshes in the simulations. The thickness of the first near-wall cell remains below one in y^+ unit, required by an LES to produce an accurate near-wall information.

Computations use no-slip boundary conditions on solid walls. The Von-Neumann boundary condition is employed for the pressure at solid walls. At the outflow boundary, a non-reflective convective boundary condition $\partial \bar{u}_i/\partial t + U_c\, \partial \bar{u}_i/\partial x = 0$ is imposed, ensuring that the flow leaves the computational domain. The convection speed U_c is set equal to the exit mean-velocity integrated across the exit plane. For the inlet flow condition, a separate LES computation for a periodic channel/pipe flow with a length of $12D_{in}$ (D_{in} is the inlet slot-height/diameter) is performed using the mass-flux and Reynolds number identical to that of the channel/pipe upstream of the flow geometry. The spacing in the inlet duct matches the grid of the corresponding channel/pipe flow simulation which creates the inflow data. The dimensionless time step $\Delta t U_{in}/D_{in}$ is tuned in a way to ensure that the Courant–Friedrichs–Lewy (CFL) number falls in a range of 0.1–0.6; this satisfies the required stability criteria in numerical schemes. Flow statistics are obtained with a desired convergence (i.e., statistically steady-state flow) and the averaging is performed over 800–1000 dimensionless time steps. In order to save CPU time, a k–ϵ model [15] is used to calculate each case with the respective grid. Afterwords, the LES starts from the results of the k–ϵ model. The time-averaging is employed to obtain the mean value of computed parameters, such as averaged velocity, temperature and turbulence kinetic energy.

3.1 Forced convection

The forced convection flow is encountered in ventilated rooms when the buoyancy effect is negligible. Computations use the experimental setting of Nielsen et al. [26] as shown in Fig. 1. The experiment considers a scale model to simulate the indoor air-flow with $W/H = 1$ and $L/H = 3$. The inlet slot-height $h_{in}/H = 0.056$ and the outlet slot-height $h_{out}/H = 0.16$. The slot-width of the inlet and outlet remains same as the model width. The incoming

velocity $U_{in} = 0.45$ m/s corresponding to a Reynolds number $Re = U_{in}h_{in}/\nu = 5 \times 10^3$ based on the inlet slot-height. A grid size of $200 \times 180 \times 140$ is used in the x (length), y (height) and z (width) directions, respectively. According to the grid-dependent study in Fig. 2 that shows the normalized mean velocity profile at the horizontal $y/H = 0.972$ location using the RAST turbulence model on three grids. This selected grid size has produced fairly accurate results compared with the fine grid with a size of $220 \times 200 \times 160$; the increased resolution does not show any noticeable differences/improvements. The DSM shows similar/smaller grid sensitivities. The mesh spacing is refined in the near-wall regions in order to capture all flow features. A dimensionless time step $\Delta t U_{in}/h_{in} = 0.001$ is used in this simulation. The time-averaging is performed when a statistical convergence is achieved. The averaging procedure is carried out for 1000 dimensionless time steps.

The normalized mean velocity and fluctuation profiles at two horizontal $y/H(= 0.028, 0.972)$ and two vertical $x/H(= 1, 2)$ locations are presented in Figs. 3 and 4, respectively. As shown in Fig. 3a, b, the predicted results agree well with the experimental data; however, the RAST model shows a better agreement with measurements as the flow travels away from the inlet. Figure 3c, d portrays the mean velocity distribution at $x/H = 1$ and $x/H = 2$, respectively. As can be seen, the RAST model predictions agree well with the experimental data close to the near-wall region due to its sensitivity to the recirculation and streamline curvature. Note that for $\bar{S} \neq \overline{W}$, Eq. (13) resembles the approach to enhancing the sensitivity of the turbulence model to streamline curvature that provokes an extra rate of strain in the flow field besides the main strain-rate. On the contrary, the sub-grid scale (SGS) viscosity of DSM is under-predicted close to the top wall (the jet region) and consequently, the mean velocity is over-predicted in that location. Overall, the trend and magnitude of predicted velocities are better predicted by the RAST model than those of the DSM when compared with the experiment.

The consequence of predicting the incorrect level of SGS viscosity is also reflected in predicted root-mean-square (RMS) velocity fluctuations as shown in Fig. 4. Probably, this would allow to identify the reasons for discrepancies between the computed results and measured data. The under-estimation of SGS eddy-viscosity implies a lower turbulence level, and the over-estimation of SGS eddy-viscosity leads to a higher turbulence level. On the whole, the RAST model gives fair results relative to the DSM in predicting the turbulence statistics when compared with experiments.

3.2 Mixed convection

The present investigation refers to a mixed convection which is a common case in a room-ventilating system, as shown in Fig. 5. The numerical simulation is based on the experimental work of Blay et al. [27], wherein the air velocity, temperature and turbulence kinetic energy are measured. Figure 5 shows that the geometry is similar to the forced convection case with the dimensions of $H = 1.04$ m high, $L = 1.04$ m long and $W = 0.7$ m wide, respectively. Again, this is a scale model of a room with the inlet slot-height $h_{in} = 0.018$ m and the outlet slot-height $h_{out} = 0.024$ m. The inlet velocity $U_{in} = 0.57$ m/s and temperature $T_{in} = 15\,^{\circ}\text{C}$ according to the experiment with $Re = 678$. The model has a floor heating system that maintains the floor temperature of $T_f = 35\,^{\circ}\text{C}$; all other walls

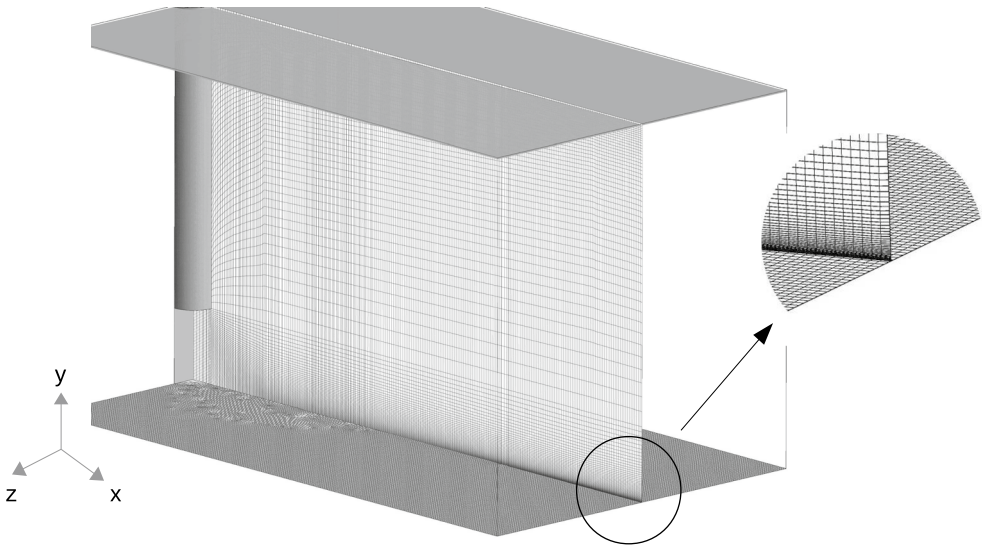

Fig. 12 Mesh distribution for impinging jet in a room

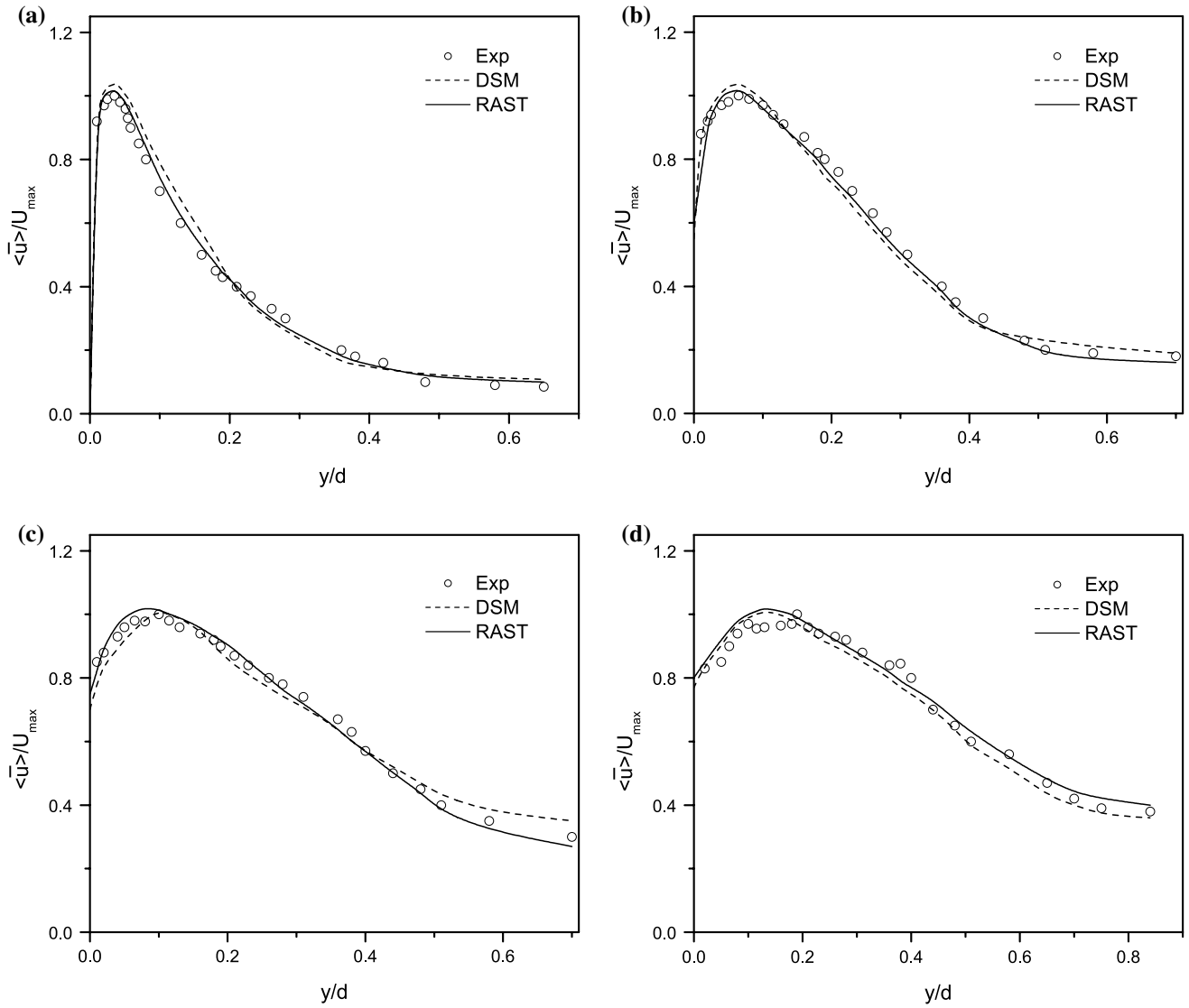

Fig. 13 Mean velocity profiles for impinging jet. **a** $x = 0.3$ m, **b** $x = 0.5$ m, **c** $x = 0.7$ m, **d** $x = 1$ m

are kept at a temperature of $T_w = 15\,^{\circ}\mathrm{C}$. Figure 6 shows the mean velocity profile at the center section $x/L = 0.5$ using the RAST turbulence model on three grids. Grids are named as coarse with $120 \times 120 \times 100$, medium with $160 \times 160 \times 120$ and fine with $200 \times 180 \times 120$ hexahedral cells, respectively. As can be seen, there is a little difference between the medium and fine grid results. The grid-sensitivity of DSM is almost analogous to that of the RAST model. Therefore, the meshes employed are $160 \times 160 \times 120$ for the x, y and z directions, respectively. The mesh is stretched in wall-normal directions with a factor of 1.05. A time step of $\Delta t U_{in}/h_{in} = 0.001$ is used, resulting in a maximum Courant (CFL) number of around 0.5. Computations are run for 1000 time steps to make sure that the flow is statistically converged.

Figure 7 compares the predicted mean air velocity distributions using the RAST model and DSM with the experimental data at two center sections $x/L = 0.5$ and $y/L = 0.5$, respectively. The predicted velocity profiles agree reasonably well with the experimental data. However, the RAST model performs slightly better than that of the DSM. Figure 8 illustrates the computed total turbulence kinetic energy at the same sections mentioned above and the comparison with the corresponding experimental data. Evidently, the shape of predicted turbulence kinetic energy profiles is the same as the measured one. Figure 9 compares further the predicted mean temperature profiles with the measured data at the above-mentioned sections. As can be seen, both SGS models give almost identical temperature distributions compared with the experiment.

3.3 Ventilation with isothermal impinging-jet

The impinging-jet ventilation system combines positive aspects of conventional mixing and displacement ventilation systems, having the potentiality for proving a better air distribution and energy-efficient operation, as well as its flexibility for both cooling and heating purposes. This method enables the air-jet to overcome the buoyancy force generated from different heat sources and reach further regions; therefore, a more efficient ventilation in the occupied zone can be achieved compared with a displacement ventilation system. Impinging jet has been widely used with various flow configurations [28]. The impinging-jet flow is characterized by a combination of three regions: free jet region, impingement region and wall jet region, as illustrated in Fig. 10. This setting has been used in the experimental study of Chen et al. [29]. The physical model under consideration is a semi-confined room with the dimensions of 5.76 m × 3.04 m × 3 m. There are three outlets (openings) inside the room; two of them are 1 m high and 5.76 m long, located beneath the two side walls. The third one (door) is placed at the end of the room with the dimensions of 3 m high and 1.32 m wide. The air is injected from a semi-elliptic pipe with a hydraulic diameter of $d = 0.1265$ m and an area of 0.0166 m^2 at a height of $h = 0.6$ m above the floor. The geometry and dimension of the supply duct at the outlet are also shown in Fig. 10.

The supplied air velocity $V_{in} = 1.2$ m/s. The inlet condition is produced from a separate calculation of a fully developed turbulent pipe flow with the same diameter to achieve a more realistic boundary condition at the exit of the nozzle. Three different non-uniform grid distributions

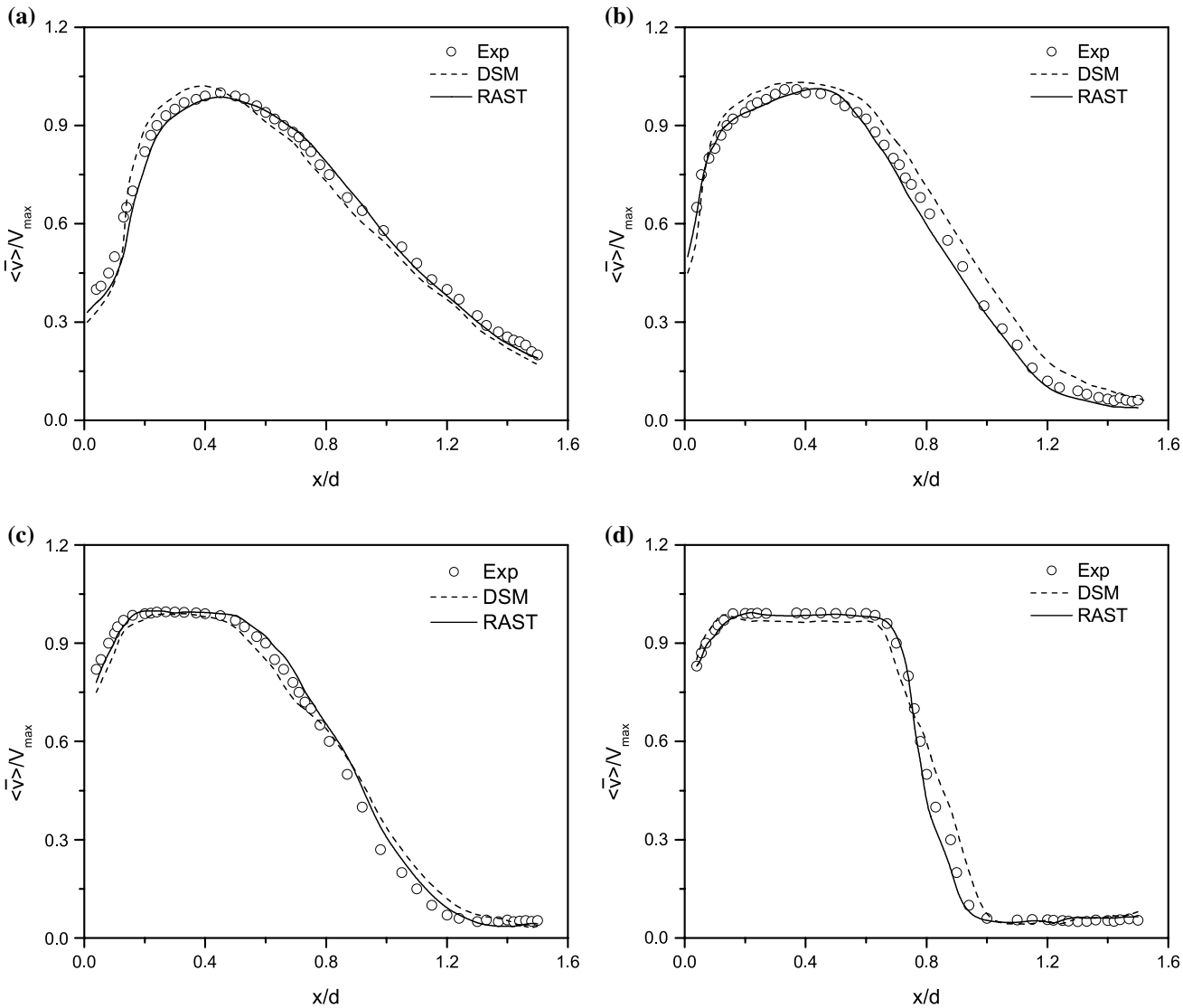

Fig. 14 y-component velocity at different location below the inlet. **a** $y = 0.065$ m, **b** $y = 0.125$ m, **c** $y = 0.225$ m **d** $y = 0.545$ m

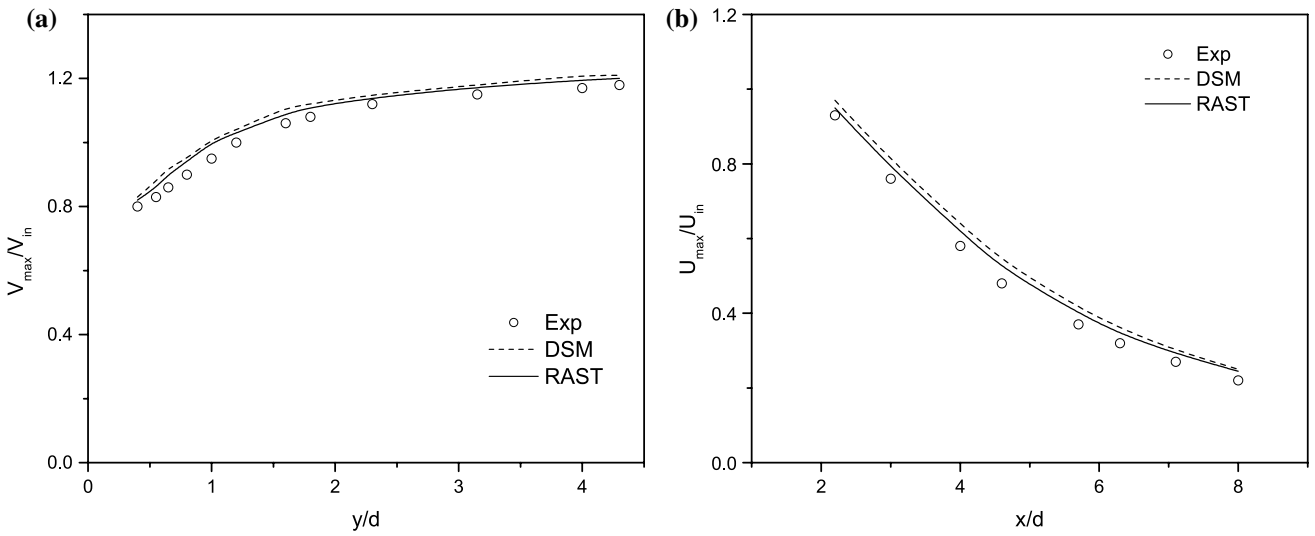

Fig. 15 Jet maximum velocity decay at different locations. **a** below inlet, **b** centerline of floor

with $4 \times 10^6, 6.5 \times 10^6$ and 8×10^6 cells respectively, are applied to investigate the grid-independency. Numerical results shown in Fig. 11 demonstrate that the predictions of last two grids are close to each other; therefore, the grid size with 6.5×10^6 cells is utilized for further validations. The grid density with $y^+ < 1$ near the wall is presented in Fig. 12. A time step of $\Delta t U_{in}/d = 0.001$ is used in the calculations. As the simulations reach a statistically steady-state, the time-averaging is performed over 800 dimensionless time steps.

Figures 13 and 14 compare the jet velocity distributions computed from the RAST model and DSM with measurements [29]. Results are analyzed at various locations in the vertical middle plane, including the regions below the inlet and along the floor. The velocity profile is normalized by its local maximum velocity U_{max} or V_{max} and the distance x or y is scaled with a hydraulic diameter $d = 0.1265$ m. To analyze the wall-jet behavior along the floor is more substantial for validating the turbulence model. The comparisons are made at four downstream distances from the inlet wall and presented in terms of the mean velocity distributions in Fig. 13. Moving from the inlet wall, the predicted velocity profiles from both tested models appear to agree well with the experimental data. In general, a better consistency is observed from the RAST model over the entire compared regions. Figure 14 exhibits the jet profiles below the inlet; the predicted jet profiles show good consistency for both implemented turbulence models compared with experimental data in the region beneath the inlet, and over most of the regions. The predictions from the two models are quite similar. Nevertheless, it is worth mentioning that this flow feature is well captured by the RAST model relative to the DSM.

Figure 15 displays the jet-dynamics regarding the maximum velocity decay in the regions below the exit and along the floor. As the jet approaches the floor, the predicted decaying trends from both models are similar to the experimental findings, faithfully reproduced in Figure 15a showing that over most of compared regions the velocity decays slowly. This is because the jet is mainly affected by the turbulence shear stress. After the jet impinges on the floor, the flow turns and follows the impingement surface. At a further downstream of the impingement point, the flow spreads parallel along the floor and decelerates in the form of a thin shear layer. Figure 15b compares the simulations with experimental data concerning the jet maximum velocity decay along the centerline of the floor. As can be seen, both models are in close agreement with experiments. It seems likely that both models are capable of capturing the mean flow field of an isothermal impinging-jet in a room satisfactorily.

4 Conclusions

The current study appears with a performance-assessment of two different zero-equation SSG models: the RAST with a single grid-filter scale, and the DSM with grid-filter and test-filter scales. Unlike the DSM, the RAST model does not need any *ad-hoc* clipping/averaging for the eddy-viscosity coefficient; instead it depends non-linearly on both the rotational and irrotational strains, providing natural damping as the wall is approached. The ability-assessment of both models to better account for non-equilibrium effects, encountered in the air-flow with forced and mixed convection in a room demonstrates that the RAST model

faithfully predicts a higher level of accuracy in comparison to the DSM, leading to an improved agreement with experimental data in most of the flow cases considered in this study. Furthermore, the RAST model retains the single grid-filter feature, which in turn renders it advantageous over the DSM.

On average, the computational effort needed for the entire simulations (indoor air-flow cases) with the RAST model in the incompressible code is about (60–70) % of the cost of the DSM. Like the Smagorinsky model, the present model is relatively cheap. Naturally, the LES with RAST model has a good potential to simulate the indoor air-flow.

References

1. Chen Q (1995) Comparison of different k-ϵ models for indoor air flow computations. Numer Heat Transf Part B 28:353–369
2. Chen Q (1996) Prediction of room air motion by Reynolds-stress model. Build Environ 31(3):233–244
3. Chen Q (1997) Computational fluid dynamics for HVAC: successes and failures. ASHRAE Trans 103(Part 1):178–187
4. Luo S, Roux B (2004) Modeling of the HESCO nozzle diffuser used in IEA annex 20 experimental test room. Build Environ 39:367–384
5. Stamou A, Katsiris I (2006) Verification of a CFD model for indoor airflow and heat transfer. Build Environ 41:1171–1181
6. Zhai Z, Zhang Z, Zhang W, Chen Q (2007) Evaluation of various turbulence models in predicting airflow and turbulence in enclosed environments by CFD. Part 1: summary of prevalent turbulence models. HVAC&R Res 13(6):871–886
7. Zhang Z, Zhang W, Zhai JZ, Chen Q (2007) Evaluation of various turbulence models in predicting airflow and turbulence in enclosed environments by CFD. Part 2: comparison with experimental data from literature. HVAC&R Res 13(6):871–886
8. Cao GY, Ruponen M, Paavilainen R, Kurnitski J (2011) Modeling and simulation of the near-wall velocity of a turbulent ceiling attached plane jet after its impingement with the corner. Build Environ 46:489–500
9. Smagorinsky J (1963) General circulation experiments with the primitive equations, I. The basic experiment. Mon Weather Rev 91:99–164
10. Germano M, Piomelli U, Moin P, Cabot WH (1991) A dynamic subgrid-scale eddy viscosity model. Phys Fluids A 3:1760–1765
11. Olsson M, Fuchs L (1996) Large eddy simulation of proximal region of a spatially developing circular jet. Phys Fluids 8:2125–2137
12. Ghosal S, Lund T, Moin P, Akselvoll K (1995) A dynamic localization model for large-eddy simulation of turbulent flows. J Fluid Mech 286:229–255
13. Meneveau C, Lund T, Cabot WH (1996) A Lagrangian dynamic sub-grid scale model of turbulence. J Fluid Mech 319:315–353
14. Taghinia J, Rahman MM, Siikonen T, Agarwal RK (2014) A sub-grid scale model with non-traditional eddy-viscosity coefficient. In: 7th AIAA theoretical fluid mechanics conference. doi:10.2514/6.2014-3212
15. Rahman MM, Siikonen T (2006) An explicit algebraic Reynolds stress model in turbulence. Int J Numer Methods Fluids 52:1135–1157
16. Rahman MM, Siikonen T (2005) An eddy viscosity model with near-wall modifications. Int J Numer Methods Fluids 49:975–997
17. Nicoud F, Ducros F (1999) Subgrid-scale stress modeling based on the square of the velocity gradient tensor. Flow Turbul Combust 62:183–200
18. Vreman AW (2004) An eddy-viscosity subgrid-scale model for turbulent shear flow: algebric theory and applications. Phys Fluids 16:3670–3681
19. Moin P, Kim J (1982) Numerical investigation of turbulent channel flow. J Fluid Mech 118:341–377
20. Lilly DK (1992) A proposed modification of the Germano subgrid-scale closure model. Phys Fluids 4(3):633–635
21. Rahman MM, Miettien A, Siikonen T (1996) Modified SIMPLE formulation on a collocated grid with an assessment of the simplified QUICK scheme. Numer Heat Transf Part B 30:291–314
22. Rahman MM, Siikonen T, Miettien A (1997) A pressure-correction method for solving fluid flow problems on a collocated grid. Numer Heat Transf Part B 32:63–84
23. Majander P (2000) Developments in large eddy simulation. Report 128, Aalto University. ISBN 951-22-4861-1
24. Davidson L (2001) Hybrid LES-RANS: a combination of a one-equation SGS model and a k-ω model for predicting recirculating flows. In: ECCOMAS CFD conference, Swansen, UK
25. Krajnovic K, Davidson L (2006) A mixed one-equation subgrid model for large-eddy simulation. Int J Heat Fluid Flow 27:402–415
26. Nielsen PV, Restivo A, Whitelaw JH (1978) The velocity characteristics of ventilated room. ASME J Fluids Eng 100:291–298
27. Blay D, Mergui S, Niculae C (1992) Confined turbulent mixed convection in the presence of a horizontal buoyant wall jet. In: Chen TS, Chu TY (eds) Fundamentals of mixed convection, HTD, vol 213. ASME, New York, pp 65–72
28. Taghinia J, Rahman MM, Siikonen T (2014) Numerical investigation of twin-jet impingement with hybrid-type turbulence modeling. Appl Therm Eng 73(1):648–657
29. Chen HJ, Moshfegh B, Cehlin M (2012) Numerical investigation of the flow behavior of an isothermal impinging jet in a room. Build Environ 49:154–166